IEEE Access
Multidisciplinary | Rapid Review | Open Access Journal

Received April 1, 2017, accepted May 22, 2017, date of publication May 31, 2017, date of current version June 27, 2017.

Digital Object Identifier 10.1109/ACCESS.2017.2710160

An Improved Full-Wave Multilevel Green's Function Interpolation Method With RBF-QR Technique for Fast Field Evaluation

PENG ZHAO[1,2], (Member, IEEE), CHI HOU CHAN[3], (Fellow, IEEE), AND GAOFENG WANG[1], (Senior Member, IEEE)

[1]Key Lab of RF Circuits and Systems of Ministry of Education, Microelectronics CAD Center, Hangzhou Dianzi University, 310018 Hangzhou, China
[2]State Key Laboratory of Millimeter Waves, Southeast University, 211189 Nanjing, China
[3]State Key Laboratory of Millimeter Waves, Partner Laboratory in the City University of Hong Kong, City University of Hong Kong, Hong Kong

Corresponding author: Gaofeng Wang (gaofeng@hdu.edu.cn)

This work was supported in part by the Natural Science Foundation of China under Grant 61601163 and Grant 61331007, in part by the Zhejiang Provincial Natural Science Foundation of China under Grant LQ16E070003, in part by the State Key Laboratory of Millimeter Waves under Grant K201710, and in part by the Hong Kong Research Grants Council under Grant CityU 11200514.

ABSTRACT An improved full-wave multilevel Green's function interpolation method (MLGFIM) with RBF-QR technique is proposed for the fast evaluation of electromagnetic field. The difficulty in applying the interpolation approach with radial basis functions (RBFs) lies in solving the increasingly singular matrix equation with the increase of the number of interpolation points. The compromise of making the basis functions relatively less smooth was used in the previous RBF implementations to address this problem. In this paper, a new interpolation scheme, the RBF-QR technique is applied to the interpolation of Green's function to resolve the ill-conditioning issue without such a compromise. A better conditioned basis function is generated by the QR-factorization technique, and it also solves the sensitivity of the basis function to the value of shape parameter. Moreover, a new hybrid interpolation pattern is adopted to optimize the grid pattern, e.g., reduce the number of interpolation points required and the boundary interpolation errors. The employment of the proposed RBF-QR technique in conjunction with hybrid interpolation pattern makes the efficiency of the MLGFIM greatly improved. The proposed algorithm is used for the analysis of problems involving objects, such as patch arrays, photonic bandgap structures, metasurface structures, double negative metamaterial and so on. Five numerical examples are given to validate this new algorithm, and show the accuracy and efficiency of the improved MLGFIM.

INDEX TERMS Fast integral equation solver, Green's function interpolation, radial basis functions, ill-condition.

I. INTRODUCTION

The ability of fast evaluation of electromagnetic field in the microwave and optical components such as patch antenna arrays, metasurface structures, or photonic bandgap structures is the key to a simulation tool. These problems are often analyzed using integral equation-based computational techniques, e.g., the method of moment (MoM) [1]. However, the computational requirements for MoM are very high, so various fast numerical methods have been proposed to accelerate the computation. For instant, multilevel fast multipole algorithm (MLFMA) [2]–[4], precorrected FFT (PFFT) [5], [6], adaptive integral method [7], [8], and sparse matrix canonical grid (SMCG) [9], [10], to name a few. All of these algorithms have a computational complexity of $O(N \log N)$, because the far-field interactions are indirectly computed using some approximation methods.

Specifically, a kernel independent approach which is called the multilevel Green's function interpolation method (MLGFIM) has been developed to solve quasi-static [11], [12] and full-wave [13], [14] electromagnetic problems. For the full-wave problems, accounting for the rapidly changing phase term of the full-wave Green's function, it is found that the Lagrange interpolation which has been adopted in quasi-static solver is no longer valid. This problem is alleviated by applying inverse multiquadric (IMQ) radial basis functions (RBFs) [15] with

staggered Tartan grid [11]. Recently, in order to enhance the efficiency of the MLGFIM, the effect of different types of RBFs has been comprehensively compared. The results show that the accuracy and efficiency of Gaussian (GA) [16] and Bessel (BE) [17] RBFs are better than that of IMQ RBFs. In addition, a modified staggered Tartan grid, which replaces the original staggered Tartan grid [13], is also proposed in [16] to obtain a better interpolation performance for the Green's function approximation. However, the previously used interpolation methods have difficulties in the orthogonalization of the RBFs, because an increasingly singular matrix equation needs to be solved with the increase of the number of interpolation points [13]. Making the basis functions relatively less smooth was used in the previous RBF implementations to alleviate the ill-conditioning issue. But less smooth RBFs will also lower the interpolation accuracy [18], [19].

Meanwhile, uniform grid pattern (e.g., staggered tartan grid [13] or modified staggered tartan grid [16]) restricts the number of interpolation points to some fixed numbers. The number of interpolation points cannot be chosen arbitrarily, and thus, redundant interpolation points should be employed to ensure the interpolation accuracy. Moreover, RBF implementation using a (quasi) uniform grid pattern leads to large errors near the boundaries of the interpolation region [20], and it will contaminate the solution and make the final results inaccurate. Hence, an interpolation pattern, which can flexibly choose the number of interpolation points and suppress the boundary errors, is required.

In this paper, a multilevel RBF-QR interpolation method is adopted for the Green's function interpolation. We adopt the QR-factorization technique suggested in [18] for the implementation of RBF interpolation, in which a better conditioned interpolation basis is generated after the factorization of the coefficient matrix of GA RBFs. Given this new basis function which removes the ill-conditioning issue, an accurate interpolation result can be obtained even the RBFs are very smooth. Moreover, to further enhance the interpolation efficiency, a new hybrid interpolation pattern which combines the modified staggered Tartan grid [16] and clustered Halton points [21] is also proposed in this paper to remedy the weakness of the previously used grid patterns. By applying this hybrid pattern, the number of interpolation points can be an arbitrary number, and no redundant interpolation points are thus required. In addition, the boundary errors are greatly suppressed, because the interpolation points are denser near the boundary for this new interpolation pattern. The proposed method involving a better conditioned basis function and a new hybrid pattern will be used to enhance the efficiency of the MLGFIM. Five numerical examples will be given to validate the accuracy and show the efficiency of the improved MLGFIM.

II. THE IMPLEMENTATION OF MLGFIM

For composite metallic and dielectric bodies, Poggio-Miller-Chang-Harrington-Wu-Tsai (PMCHWT) [22] integral equations are frequently used to describe this problem. After

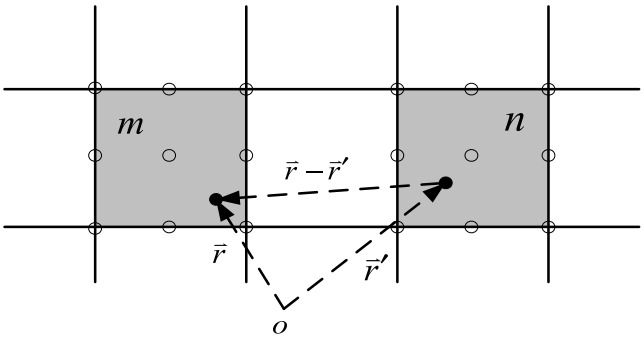

FIGURE 1. 2-D pictorial representation of the interpolation points (white circles) and interpolated points (black circles) in the field group *m* and source group *n*.

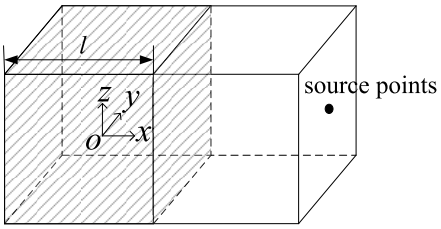

FIGURE 2. The testing scheme in which the interpolation points are distributed in the slash group and the source point locates one group length away from the slash group.

applying the Galerkin method to the integral equations, a corresponding matrix equation is generated, and each matrix element can be expressed into the scalar form as [14]:

$$Z_{ij}^{(v)} = \alpha \int_{s_i^{(v)}} ds \int_{s_j^{(v)}} ds' \tau_i(\vec{r}) \varsigma_j(\vec{r}') \Lambda^{(v)}(\vec{r}, \vec{r}') \qquad (1)$$

where α is a constant, $\Lambda^{(v)}(\vec{r}, \vec{r}')$ is the interaction function between field point $\vec{r}$ and source point $\vec{r}'$, and $\tau_i(\vec{r})$ and $\varsigma_j(\vec{r}')$ are related to the weighting function and the basis function.

In order to efficiently solve the matrix equation generated by the integral equations, MLGFIM is applied to accelerate the matrix-vector multiplication. With multilevel division, the under-simulated structure is divided and enclosed into groups. Instead of directly calculating interaction function, MLGFIM uses interpolation method to quickly approximate this function if these two groups are far apart. In order to illustrate the interpolation approximation of the interaction function, we consider the scenario in Fig. 1. According to [11], the interaction function $\Lambda^{(v)}(\vec{r}, \vec{r}')$ between field group m and source group n can be approximated using interpolation approach as follows:

$$\Lambda^{(v)}(\vec{r}, \vec{r}') = \sum_{p=1}^{N} \sum_{q=1}^{N} \omega_{m,p}(\vec{r}) \omega_{n,q}(\vec{r}') \Lambda^{(v)}(\vec{r}_{m,p}, \vec{r}'_{n,q}) \qquad (2)$$

where $\omega_{m,p}(\vec{r})$ and $\omega_{n,q}(\vec{r}')$ are the pth and qth interpolation functions, $\vec{r}_{m,p}$ and $\vec{r}'_{n,q}$ are the pth and qth interpolation

points in field group m and source group n, respectively. N is the number of interpolation points.

After substituting (2) into (1), we can implement the MLGFIM to accelerate the computation, viz.,

$$Z_{ij}^{(v)} = \alpha \left[\int_{s_i^{(v)}} ds \tau_i(\vec{r}) \bar{\omega}_m^T(\vec{r}) \right] \overline{\overline{\Lambda}}_{mn}^{(v)} \left[\int_{s_j^{(v)}} ds' \varsigma_j(\vec{r}') \bar{\omega}_n(\vec{r}') \right] \quad (3)$$

where $\bar{\omega}_m^T(\vec{r})$ is the interpolation function matrix consisting of $\omega_{m,p}(\vec{r})$ and $\overline{\overline{\Lambda}}_{mn}^{(v)}$ is the interaction function matrix consisting of $\Lambda^{(v)}\left(\vec{r}_{m,p}, \vec{r}'_{n,q}\right)$.

III. INTERPOLATE Green's FUNCTION WITH RBF-QR METHOD

Consider a function $f(\vec{r})$ in an influence domain that has a set of n arbitrarily distributed nodes with corresponding values $\{f(\vec{r}_i)\}_{i=1}^N$. Applying the basis function $\varphi\left(\left|\vec{r}-\vec{r}_i\right|, s\right)$ (where s is the shape parameter), we obtain the approximation function $f_a(\vec{r})$ as [15]:

$$f_a(\vec{r}) = [\varphi_1 \cdots \varphi_N] \bar{\bar{\Phi}}^{-1} \left[f(\vec{r}_1) \cdots f(\vec{r}_N) \right]^T \quad (4)$$

where $\varphi_i = \varphi\left(\left|\vec{r}-\vec{r}_i\right|, s\right)$ and the entries of matrix $\bar{\bar{\Phi}}$ are $\Phi_{i,j} = \varphi\left(\left|\vec{r}_j-\vec{r}_i\right|, s\right)$. The matrix $\bar{\bar{\Phi}}$ becomes increasingly singular with the increase of number of interpolation points, so the inverse operation of this matrix is difficult. As we have addressed, conventional RBF interpolation alleviates the ill-conditioning problem with the compromise of the use of less smooth basis functions.

In order to deal with the ill-conditioning problem without such a compromise, RBF-QR method is applied for Green's function interpolation. With Taylor expansion and spherical-Chebyshev expansion, the GA RBFs can be rewritten as [18]:

$$\begin{aligned} \varphi_i &= e^{-(s|\vec{r}-\vec{r}_i|)^2} \\ &= \sum_{j=0}^{j_{tru}} \sum_{m=0}^{(j-p)/2} d_{j,m} \sum_{v=-(2m+p)}^{2m+p} c_{j,m,v}(\vec{r}_i) \cdot T_{j,m,v}(\vec{r}) \end{aligned} \quad (5)$$

where $p = \mathrm{mod}(j, 2)$ and j_{tru} is the number of terms of the truncated Taylor expansion. Other coefficients in function (5) are defined as

$$d_{j,m} = 2^{3+p+4m} s^{2j} \frac{((j+p+2m)/2)!}{((j-p-2m)/2)!(j+1+p+2m)!} \quad (6)$$

$$\begin{aligned} c_{j,m,v}(\vec{r}_i) = t_{j-2m} y_v e^{-s^2 R_i^2} r_i^j Y_{2m+p}^v(\theta_i, \phi_i)\, {}_2F_3 \\ \times \left(\rho_{j,m}, \sigma_{j,m}, s^4 R_i^2\right) \end{aligned} \quad (7)$$

$$T_{j,m,v}(\vec{r}) = e^{-s^2 R^2} r^{2m} Y_{2m+p}^v(\theta, \phi)\, T_{j-2m}(R) \quad (8)$$

where

$$\begin{cases} Y_\mu^v(\theta,\phi) = P_\mu^v(\cos\theta)\cos(v\phi), v = 0, \cdots, \mu \\ Y_\mu^{-v}(\theta,\phi) = P_\mu^v(\cos\theta)\sin(v\phi), v = 1, \cdots, \mu \end{cases} \quad (9)$$

$$\begin{cases} \vec{r} = r\left(\sin\theta\cos\phi\hat{x} + \sin\theta\sin\phi\hat{y} + \cos\theta\hat{z}\right) \\ \vec{r}_i = r_i\left(\sin\theta\cos\phi\hat{x} + \sin\theta\sin\phi\hat{y} + \cos\theta\hat{z}\right) \end{cases} \quad (10)$$

$$\rho_{j,m} = [(j-2m+1)/2, (j-2m+2)/2] \quad (11)$$

$$\sigma_{j,m} = [j-2m+1, (j-2m-p+2)/2, (j+2m+p+3)/2] \quad (12)$$

and $y_0 = 0.5$, $y_v = 1 (v > 0)$, $t_0 = 0.5$, $t_{j-2m} = 1 (j > 2m)$. $P_\mu^v(x)$, $T_n(x)$ and ${}_2F_3(x)$ are the normalized associated Legendre function, Chebyshev polynomial of the first kind and hypergeometric function, respectively.

Considering the RBFs centered at N different points, the following relation is obtained according to the expansion (5):

$$\begin{bmatrix} \varphi_1 \\ \varphi_2 \\ \vdots \\ \varphi_N \end{bmatrix} = \begin{bmatrix} c_{0,0,0}(\vec{r}_1) & c_{1,0,-1}(\vec{r}_1) & \cdots & c_{j_{tru},(j_{tru}-p)/2,j_{tru}}(\vec{r}_1) \\ c_{0,0,0}(\vec{r}_2) & c_{1,0,-1}(\vec{r}_2) & \cdots & c_{j_{tru},(j_{tru}-p)/2,j_{tru}}(\vec{r}_2) \\ \vdots & \vdots & \ddots & \vdots \\ c_{0,0,0}(\vec{r}_N) & c_{1,0,-1}(\vec{r}_N) & \cdots & c_{j_{tru},(j_{tru}-p)/2,j_{tru}}(\vec{r}_N) \end{bmatrix} \cdot \begin{bmatrix} d_{0,0} & 0 & \cdots & 0 \\ 0 & d_{1,0} & \cdots & 0 \\ \vdots & \vdots & \ddots & \vdots \\ 0 & 0 & \cdots & d_{j_{tru},(j_{tru}-p)/2} \end{bmatrix} \cdot \begin{bmatrix} T_{0,0,0}(\vec{r}) \\ T_{1,0,-1}(\vec{r}) \\ \vdots \\ T_{j_{tru},(j_{tru}-p)/2}(\vec{r}) \end{bmatrix} \quad (13)$$

or

$$\bar{\Psi} = \bar{\bar{C}} \cdot \bar{\bar{D}} \cdot \bar{T}(\vec{r}) \quad (14)$$

By QR-factorizing the rectangular coefficient matrix $\bar{\bar{C}}$, equation (14) can be expressed as:

$$\begin{aligned} \bar{\Psi} &= \bar{\bar{Q}} \cdot \bar{\bar{R}} \cdot \bar{\bar{D}} \cdot \bar{T}(\vec{r}) = \bar{\bar{Q}} \cdot \begin{bmatrix} \bar{\bar{R}}_1 & \bar{\bar{R}}_2 \end{bmatrix} \begin{bmatrix} \bar{\bar{D}}_1 & 0 \\ 0 & \bar{\bar{D}}_2 \end{bmatrix} \cdot \bar{T}(\vec{r}) \\ &= \bar{\bar{Q}} \cdot \begin{bmatrix} \bar{\bar{R}}_1\bar{\bar{D}}_1 & \bar{\bar{R}}_2\bar{\bar{D}}_2 \end{bmatrix} \cdot \bar{T}(\vec{r}) \end{aligned} \quad (15)$$

where $\bar{\bar{R}}_1$ is upper triangular and both $\bar{\bar{R}}_1$ and $\bar{\bar{D}}_1$ are $N \times N$.

It has been proven that the expansion functions $T_{j,m,v}(\vec{r})$ are better conditioned and insensitive to the shape of RBFs [18], changing the basis function to be more similar to the expansion functions can resolve the ill-conditioning problem. Hence, a new basis is generated as [18]:

$$\begin{aligned} \bar{\chi} &= \bar{\bar{D}}_1^{-1}\bar{\bar{R}}_1^{-1}\bar{\bar{Q}}^H\bar{\Psi} = \begin{bmatrix} \bar{\bar{I}} & \bar{\bar{D}}_1^{-1}\bar{\bar{R}}_1^{-1}\bar{\bar{R}}_2\bar{\bar{D}}_2 \end{bmatrix} \cdot \bar{T}(\vec{r}) \\ &= \begin{bmatrix} \bar{\bar{I}} & \bar{\bar{R}}' \end{bmatrix} \cdot \bar{T}(\vec{r}) \end{aligned} \quad (16)$$

which can be viewed as the expansion functions $\bar{T}(\vec{r})$ plus a correction part. With this new basis, we can also obtain approximation function $f_a(\vec{r})$ using equation (4).

To validate the effect of the RBF-QR method, the same testing scheme introduced in [13], [16], [17], [23] is used and also shown in Fig. 2. The source point is one group length away from the field group (slash) and located at the face center (black dot). It has been proven that (quasi-uniform) Halton points are appropriate for RBF interpolation, and if these quasi-uniform points are clustered towards the domain boundary, better interpolation accuracy will be

achieved [18], [20]. Thus, we distribute the interpolation points in the field group with the length of l as:

$$\tilde{\alpha}_i = \frac{l}{2} \cdot \sin(\pi \cdot \alpha_i / l), \quad \alpha_i = x_i, y_i \text{ or } z_i \tag{17}$$

where x_i, y_i and z_i are the Cartesian coordinates of i-th Halton points [21]. The grid generated by equation (17) is clustered similarly to Chebyshev grid without being restricted to specific locations.

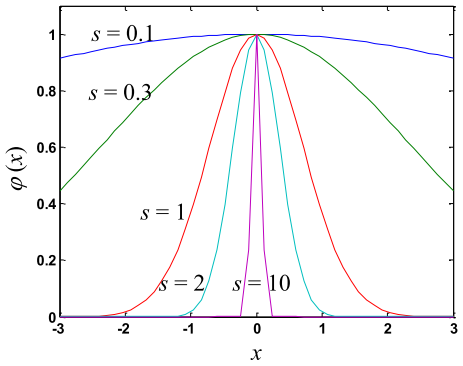

FIGURE 3. The 1-D GA RBFs using five different shape parameters.

The condition number and maximum interpolation error in the field group with different number of clustered Halton points and shape parameter s are tested. The shape parameter s controls the shape of basis function, as shown in Fig. 3. It is observed that as s reduces, the smoothness of the GA RBF increases. When the value of s reduces to a relatively small number, the GA RBF becomes almost linear near the center, and consequently eliminates the coordinate dependence. The entries in the coefficient matrix are hard to distinguish and the ill-conditioning problem occurs. So that a lot of numerical cancellation occurs when evaluating $f_a(\vec{r})$. On the other hand, if the value of s is large, the derivative of basis function becomes discontinuous at the center. Thus, a large shape parameter does not give very smooth interpolates and is generally not preferred [19]. This phenomenon suggests that computations for smaller values of ε can be very accurate if the conditioning problem is overcame by applying the new basis function (16).

Figs. 4(a) and (b) show the condition number and maximum interpolation error when the shape of the RBF is fixed. The shape parameter is set as $s = 0.2$, which implies that a smooth basis function is used. When the edge length of the testing group l is $l = 1\lambda$, the interpolation performance using RBF-QR method and conventional RBF method based on GA RBFs are compared. From Fig. 4(a), it is observed that when the number of interpolation points increases, the condition number for conventional RBF method increases accordingly and consequently causes ill-conditioning problem. However, since a better conditioned basis (16) is adopted, the condition number for RBF-QR method is much smaller. The maximum interpolation error shown in Fig. 4(b) indicates that conventional RBF method results in large interpolation error after the

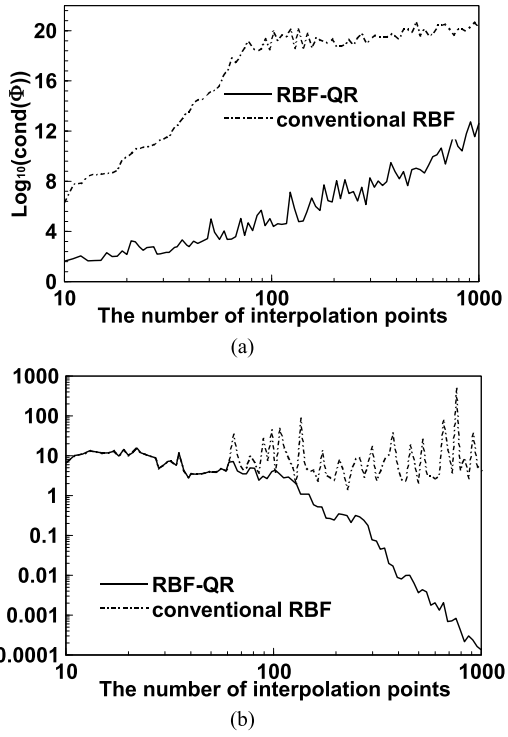

FIGURE 4. The interpolation results when $l = 1\lambda$ and $s = 0.2$. (a) Logarithm (base 10) of the condition number for matrix $\bar{\bar{\Phi}}$. (b) Maximum interpolation error.

number of interpolation points N increases beyond 70. In contrast, owing to the great reduction of condition number, the interpolation using RBF-QR method becomes increasingly accurate with the increase of the number of interpolation points.

The interpolation performances using RBFs with different shape parameters are shown in Figs. 5(a) and (b). The number of clustered Halton points N in this figure is set as $N = 300$. From these two figures, it is observed that when the value of shape parameter s is small (corresponding to flat and smooth RBFs in Fig. 3), the condition number using conventional RBF method is very large, and consequently generates inaccurate interpolation results. Increasing the value of shape parameter alleviates this problem and reduces the interpolation errors. But when the shape parameter increases beyond 1.8, the interpolation errors increase again due to the discontinuous derivative of the basis function. Since the better conditioned basis (16) is insensitive to the value of shape parameter, the condition number of matrix $\bar{\bar{\Phi}}$ for RBF-QR method remains small and changes little with the variation of shape parameter values. As a result, the interpolation accuracy using RBF-QR method is always smaller than that using conventional RBF method until the shape parameter increases to 1.8, and then the interpolation errors become the same.

IV. APPLYING A HYBRID INTERPOLATION PATTERN

Although the staggered Tartan grid (STG) [13], [16] performs better than clustered Halton points in the Green's function

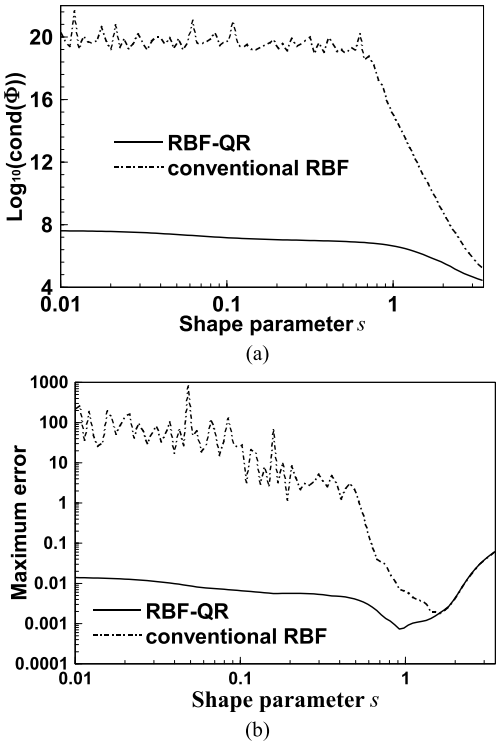

FIGURE 5. The interpolation results when $l = 1\lambda$ and $N = 300$. (a) Logarithm (base 10) of the condition number for matrix $\bar{\bar{\Phi}}$. (b) Maximum interpolation error.

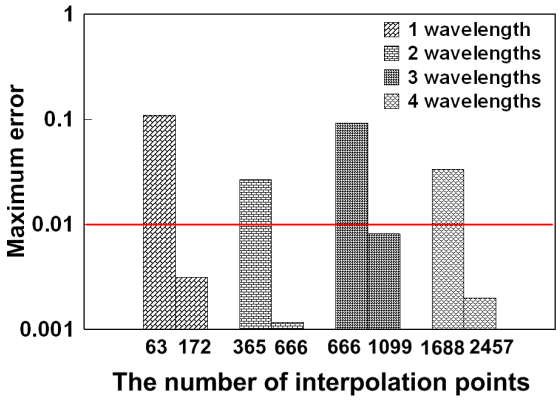

FIGURE 6. The maximum interpolation error for staggered grid points (two adjacent specific numbers of staggered points are shown in the figure).

interpolation, the restriction of these grid patterns which has been addressed involves the use of some redundant interpolation points. Fig. 6 shows the maximum interpolation error for different group lengths when STG is applied. Since the interpolation results in the testing group are uneven in accuracy, and the part with large interpolation errors will contaminate the solution everywhere across the domain, a threshold of maximum interpolation error should be set to ensure the accuracy of MLGFIM. In this paper, the error threshold E_{thre} is set as $E_{thre} = 0.01$. From Fig. 6, we find

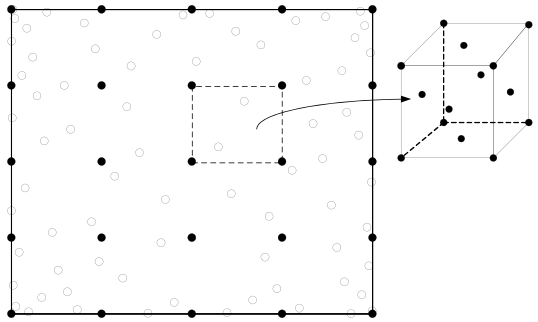

FIGURE 7. 2-D representation of a 3-D hybrid pattern (solid dots and hollow dots are staggered grid points and cluster Halton points, respectively).

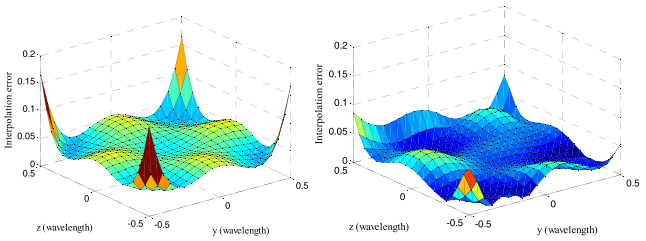

FIGURE 8. The distributions of interpolation errors when $l = 1\lambda$ and $x = -0.4\lambda$ using (a) staggered grid pattern and (b) hybrid pattern.

that we must use 172 staggered grid points to satisfy the error threshold when the edge length of group $l = 1\lambda$. Actually, to satisfy the error threshold, the number of interpolation points required is between 63 and 172. Since it is impossible to generate the number of staggered grid points between 63 and 172, some redundant interpolation points must be used.

The clustered Halton points have no such a restriction, and thus it is possible to remedy the weakness of staggered grid by combining it with clustered Halton points. The hybrid interpolation pattern, as shown in Figure 7, is generated as follows. Assume the edge length of group $l = 1\lambda$, it has been inferred that the actual number of interpolation points is between 63 and 172. Hence, 63 staggered grid points are first adopted to compose one part of the hybrid pattern. Subsequently, the clustered Halton points generated by (17) are gradually added to the hybrid pattern until the maximum error using the total interpolation points is below the threshold.

Apart from the above advantage, the hybrid interpolation pattern can also suppress the boundary interpolation errors. Assume the edge length of group l is chosen as $l = 1\lambda$ and 63 staggered grid points are used for the interpolation. Fig. 8(a) shows the distribution of interpolation errors on the plane that is close to the edges of the group ($x = -0.4\lambda$). From Fig. 8(a), it is observed that the interpolation errors near the corners are very large, and that makes the interpolation at these regions inaccurate. Fig. 8(b) shows the error distribution on the same plane when hybrid pattern consisting of 63 staggered grid points and 10 clustered Halton points is applied. We find that the corner errors are suppressed after only 10 clustered Halton points are augmented.

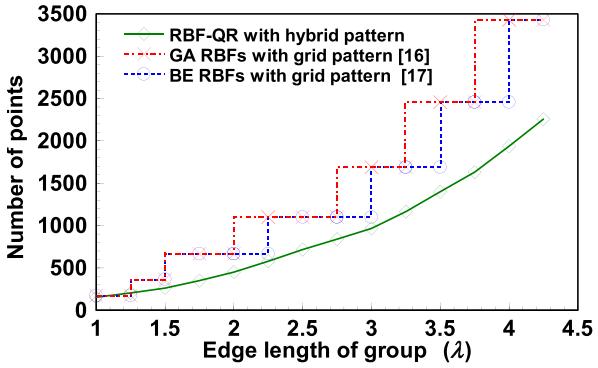

FIGURE 9. Required number of interpolation points using RBF-QR with hybrid pattern and the methods in [16] and [17].

Furthermore, the required numbers of interpolation points using the proposed method for different group lengths are given and compared with those using the previously reported methods [16] and [17], as shown in Fig. 9. The increase step of group length is set as quarter wavelength in this figure, and it is observed that the number of required interpolation points using the proposed method is always smaller than that using the previous methods.

TABLE 1. Comparison of the interpolation accuracy between RBF-QR and conventional RBF method with BE RBFs.

Interpolation method	$l(\lambda)$	STG points	Halton points	Shape parameter s	Maximum error ($\times 10^{-2}$)
RBF-QR	1.0	63	90	1.21	0.86
	2.0	365	85	0.48	0.95
	3.0	666	300	0.219	0.99
	4.0	1688	250	0.137	0.97
RBF with BE RBFs	1.0	63	90	6.70	1.12
	2.0	365	85	3.26	2.26
	3.0	666	300	2.11	2.66
	4.0	1688	250	1.58	3.63

Since the BE RBFs have a better convergence behavior than other used basis functions [17], to further prove the effectiveness of the proposed methods, the interpolation accuracy using RBF-QR method and conventional RBF method based on BE RBFs with the same number of interpolation points are compared, as shown in Table 1. From this table, we find that the interpolation accuracy of using RBF-QR method is better than that using conventional RBF method, and the difference of maximum error between these two methods are increased with the increase of the group length.

V. NUMERICAL RESULTS

In this section, three examples are given to demonstrate good performance of the proposed method. The generalized minimal residual (GMRES) iteration method with a relative error norm of 10^{-3} is employed for all the calculations, and the inner loop of GMRES contains 100 matrix-vector multiplications.

As the first example, the proposed algorithm is applied to solve the plane wave scattering from a 3 by 3 microstrip patch

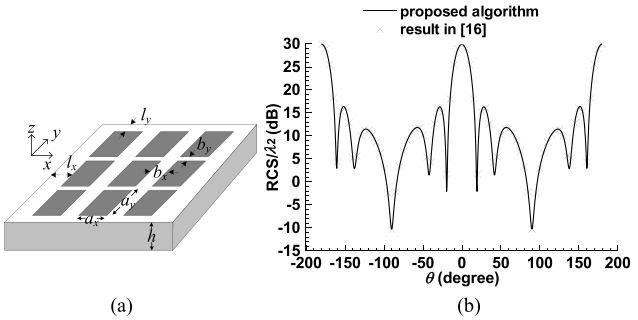

FIGURE 10. Plane wave scattering from a 3 by 3 patch array. (a) Geometry and (b) Bistatic RCS $\theta\theta$ polarization.

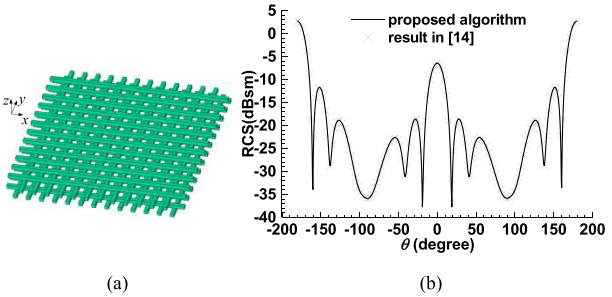

FIGURE 11. Plane wave scattering from a four-layer photonic band gap structure. (a) Geometry and (b) Bistatic RCS $\theta\theta$ polarization.

array, as shown in Fig. 10(a). The parameters of the array are as follows: $a_x = 3.66\ cm$, $a_y = 2.6\ cm$, $b_x = 1.8917\ cm$, $b_y = 2.9517\ cm$, $l_x = l_y = 5\ cm$, $h = 0.158\ cm$. The relative permittivity of the substrate is 2.17. A plane wave with center frequency of 3.7 GHz is normally incident along $-z$ axis. 12 grids per wavelength λ_d (where $\lambda_d = \lambda_0/\sqrt{\varepsilon_r}$) are used to discretize the array and the total number of unknowns for the equivalent electric and magnetic currents is 25,988. Fig. 9(b) shows the bistatic RCS with $\theta\theta$ polarization result calculated by the proposed algorithm and the result in [16]. Very good agreement is observed between two results which validates the proposed algorithm.

In the second case, plane wave scattering from a four-layer photonic band gap structure is analyzed, as shown in Fig. 11(a). The structure is made of layers of dielectric rods with an orderly stacking sequence. In each layer, 12 or 13 alumina rods with a refractive index of 3.1 are arranged parallel to each other, and separated by a center-to-center distance of 1.123 *cm*. The width, height and length of the rods are 0.318 *cm*, 0.318 *cm* and 15.24 *cm*, respectively. The rods of the second neighbor layer are shifted by 0.5615 *cm* in the direction perpendicular to the rod axes. A plane wave propagating along $-z$ axis impinges normally to the structure. The center frequency of the wave is 6.0 GHz. After discretizing the structure, 204,888 unknowns for the equivalent electric and magnetic currents are obtained. The bistatic RCS with $\theta\theta$ polarization result calculated by the proposed algorithm is shown in Fig. 11(b), and compared with the result shown in [14]. Again, good agreement is observed between these two results.

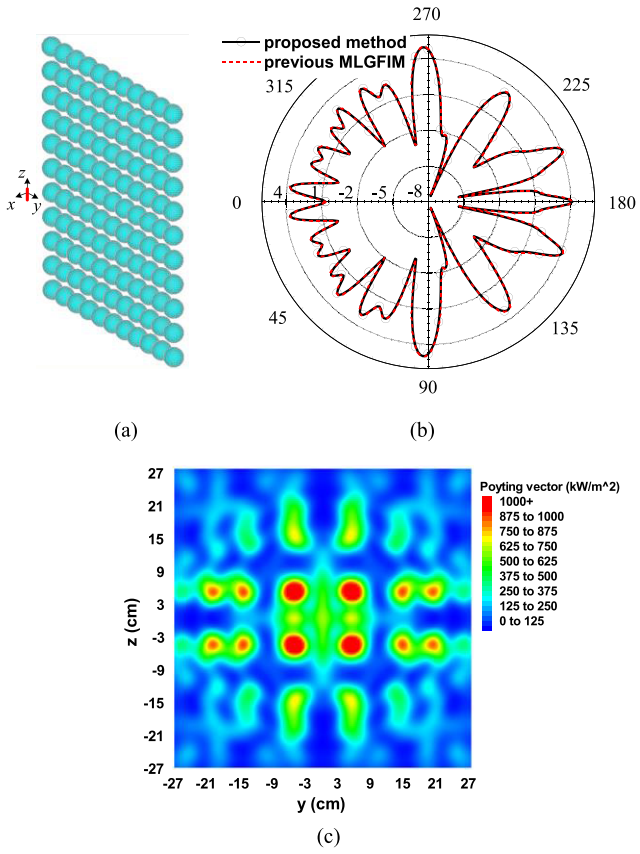

FIGURE 12. A dipole in front of an 11 by 11 dielectric sphere array. (a) Geometry. (b) Polar plot of the directivity versus ϕ in dB when $\theta = 90°$. (c) Distribution of Poynting vector in *yoz* plane.

Next, the structure of a dipole in front of an 11 by 11 dielectric sphere array ($\varepsilon_r = 2.25$) is investigated, as shown in Fig. 12(a). The radius of the sphere is 2 *cm* and the distance between the centers of two adjacent spheres is 5 c*m*. A Herzian dipole which works at the frequency of 6.25GHz is located 10 c*m* in front of the array center and placed along z axis. In this example, 10 grids per wavelength λ_d are used to discretize this structure so that the number of unknowns for equivalent electric and magnetic currents is 144,020. The polar plot of the directivity versus ϕ when $\theta = 90°$ is shown in Fig. 12(b). The results calculated by the proposed algorithm and previous MLGFIM [17] which applies BE RBFs with STG pattern are agreed very well. The distribution of Poynting vector in the plane of $x = -20$ c*m* is also calculated, as shown in Fig. 12(c).

In the following example, consider a plane wave impinges normally on a fishnet-type structure which always performances as metamaterial [24]. Fig. 13(a) shows a fishnet-type structure consisting of 10×10 elements, and its corresponding element in 3-D view, in which $w_1 = 10\ \mu$m, $w_2 = 17.5\ \mu$m, $d = 115\ \mu$m, $t = 9\ \mu$m. The patterns on the top and bottom surfaces of the substrate are made of the same shaped PEC, and the permittivity of the substrate is 2.25. A plane wave with electric field parallel to the x-axis propagates along $-$z-axis, the magnitude of the electric field

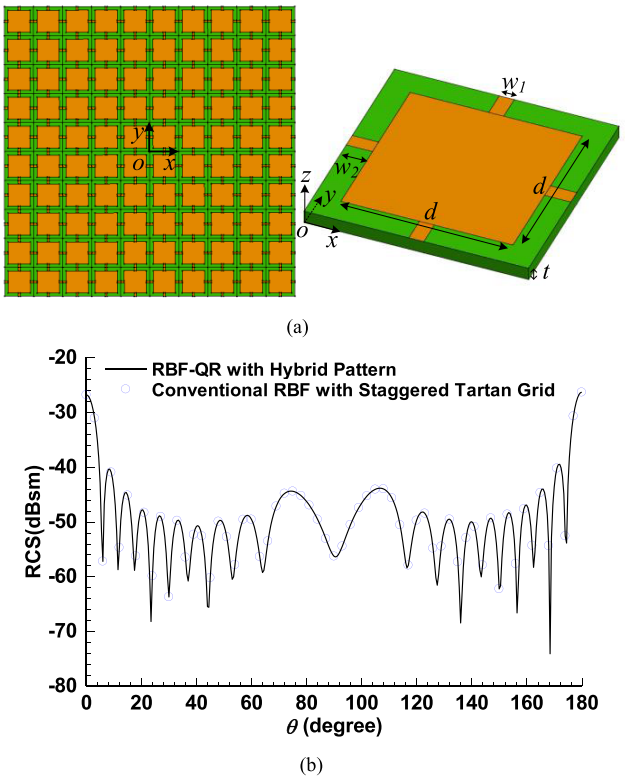

FIGURE 13. Plane wave impinges normally on a finite fishnet-type metasurface structure. (a) Geometry. (b) Bistatic RCS with $\theta\theta$ polarization.

TABLE 2. Comparison of CPU time and memory requirement.

Methods	Examples	Maximum electrical length (λ_d)	The number of unknowns	CPU time for per matrix-vector multiplication (second)	Memory (GB)
Proposed algorithm	1	4.50	25,988	13.9	0.43
	2	9.46	204,888	108.3	3.95
	3	16.87	144,020	110.9	3.45
	4	15	222,512	127.5	3.96
BE RBFs with STG [17]	1	4.50	25,988	16.3	0.48
	2	9.46	204,888	163.2	5.63
	3	16.87	144,020	256.1	6.11
	4	15	222,512	289.9	7.83

of the incident wave is 1 V/m. The bistatic RCS is investigated at the frequency of 2 THz. From Fig. 13(b), it can be seen that the results calculated by the proposed method and previous MLGFIM [17] agree very well.

We also compare the computational efficiency between the proposed algorithm and previous MLGFIM algorithm. In [17], the interpolation results show that the efficiency of BE RBFs with staggered points are better than previously used interpolation methods (including methods in [14] and [16]) for Green's function approximation. Therefore, we compare the computational performance of MLGFIM using the proposed algorithm and BE RBFs with staggered grid pattern for the aforementioned three examples, as shown in Table 2. From this table, it is observed that the CPU times for the four examples have reduced by 14.7%, 33.6%, 56.7% and

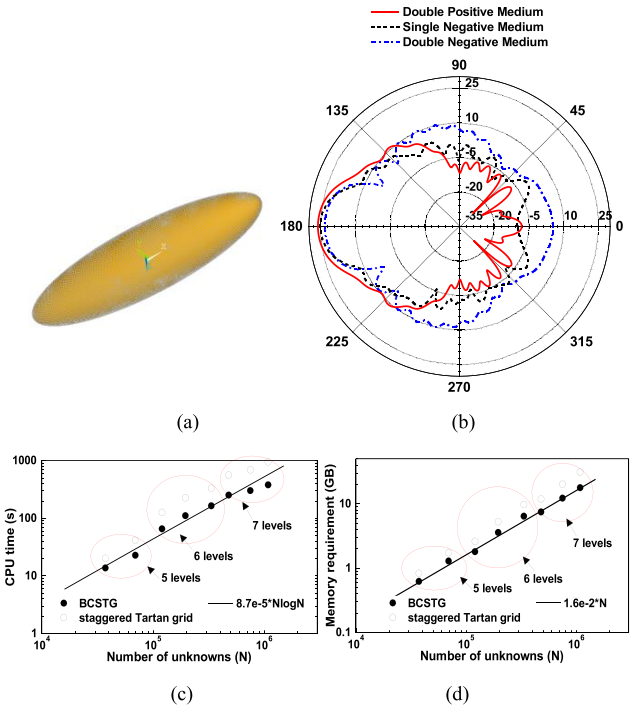

FIGURE 14. Plane wave scattering from a dielectric elliptical sphere. (a) Geometry. (b) Bistatic RCS with $\phi\phi$ polarization. (c) CPU time. (d) Memory requirement.

56.0%, respectively, after applying the proposed algorithm. It should be mentioned that because the large size of example 3 make it requires more interpolation points than example 2, although the number of unknowns in example 2 is larger than example 3, the time for simulating example 2 is still shorter. Table 2 also compares the memory requirements between the proposed method and previous MLGFIM. The comparison results show that the memory requirements have been saved by 10.4%, 29.8%, 43.5 % and 49.4% for the four examples, respectively. More significant reductions of calculation time and memory requirement can be observed with the increase of the object size.

Finally, a dielectric elliptical sphere consisting of different types of mediums is subsequently considered, as shown in Fig. 14(a). The long axis of the elliptical sphere is 6 m, whereas the short axis is 1.5 m. The plane wave scattered by this elliptical sphere comprising double positive ($\varepsilon_r = 2.25$, $\mu_r = 1.0$), single negative ($\varepsilon_r = -2.25$, $\mu_r = 1.0$) and double negative ($\varepsilon_r = 2.25$, $\mu_r = -1.0$) medium is studied. Fig. 14(b) compares the bistatic RCS with $\phi\phi$ polarization for these three cases, when plane wave with a frequency of 300 MHz is impinges on the elliptical sphere along $-x$ axis. The forward scattering is enhanced significantly due to negative permittivity and permeability. The CPU time for performing each matrix-vector multiplication and the corresponding memory requirement are shown in Figs. 14(c) and (d), in which the frequency of incident wave gradually increases. In these two figures, about 20 grids per wavelength are used to discretize this structure, and three types of numbers of levels are used for the calculation. From Fig. 14(c) and (d), it is observed that the CPU time and memory requirement of the proposed method are always smaller than those of the previous one. In addition, it is also observed that the proposed algorithm approximately obeys a computational complexity of $O(N \log N)$ and memory complexity of $O(N)$.

VI. CONCLUSION

A new interpolation scheme using RBF-QR method with hybrid interpolation pattern is proposed to improve the computational efficiency and memory storage requirement of MLGFIM. The RBF-QR method resolves the ill-conditioning problem without the compromise of adopting less smooth RBFs, and the hybrid pattern optimizes the interpolation grid pattern. Compared with previously reported schemes, this method can provide a better interpolation performance, and thus make the MLGFIM more efficient.

REFERENCES

[1] R. F. Harrington, *Field Computation by Moment Methods*. Piscataway, NJ, USA: IEEE Press, 1993.
[2] J. Song, C.-C. Lu, and W. C. Chew, "Multilevel fast multipole algorithm for electromagnetic scattering by large complex objects," *IEEE Trans. Antennas Propag.*, vol. 45, no. 10, pp. 1488–1493, Oct. 1997.
[3] J. M. Song, C. C. Lu, W. C. Chew, and S. W. Lee, "Fast Illinois solver code (FISC)," *IEEE Antennas Propag. Mag.*, vol. 48, no. 3, pp. 27–34, Jun. 1998.
[4] W. C. Chew, J. M. Jin, E. Michielssen, and J. M. Song, *Fast and Efficient Algorithms in Computational Electromagnetics*. Norwood, MA, USA: Artech House, 2001.
[5] J. R. Phillips and J. K. White, "A precorrected-FFT method for electrostatic analysis of complicated 3-D structures," *IEEE Trans. Comput.-Aided Des. Integr. Circuits Syst.*, vol. 16, no. 10, pp. 1059–1072, Oct. 1997.
[6] H. Hu *et al.*, "Fast on-chip inductance simulation using a precorrected-FFT method," *IEEE Trans. Comput.-Aided Des. Integr. Circuits Syst.*, vol. 22, no. 1, pp. 49–66, Jan. 2003.
[7] E. Bleszynski, M. Bleszynski, and T. Jaroszewicz, "AIM: Adaptive integral method for solving large-scale electromagnetic scattering and radiation problems," *Radio Sci.*, vol. 31, no. 5, pp. 1225–1251, May 1996.
[8] F. Ling, C. F. Wang, and J. M. Jin, "An efficient algorithm for analyzing large-scale microstrip structures using adaptive integral method combined with discrete complex image method," *IEEE Trans. Microw. Theory Tech.*, vol. 48, no. 5, pp. 832–837, May 2000.
[9] C. H. Chan, C. M. Lin, L. Tsang, and Y. F. Leung, "A sparse-matrix/canonical grid method for analyzing microstrip structures," *IEICE Trans. Electron. (EC)*, vol. 80, no. 11, pp. 1354–1359, 1997.
[10] S. Q. Li, Y. Yu, C. H. Chan, K. F. Chan, and L. Tsang, "A sparse-matrix/canonical grid method for analyzing densely packed interconnects," *IEEE Trans. Microw. Theory Techn.*, vol. 49, no. 7, pp. 1221–1228, Jul. 2001.
[11] H. G. Wang, C. H. Chan, and L. Tsang, "A new multilevel Green's function interpolation method for large-scale low-frequency EM simulations," *IEEE Trans. Comput.-Aided Des. Integr. Circuits Syst.*, vol. 24, no. 9, pp. 1427–1443, Sep. 2005.
[12] P. Zhao and H. G. Wang, "Resistances and inductances extraction using surface integral equation with the acceleration of multilevel Green's function interpolation method," *Prog. Electromagn. Res.*, vol. 83, pp. 43–54, 2008.
[13] H. G. Wang and C. H. Chan, "The implementation of multilevel Green's function interpolation method for full-wave electromagnetic problems," *IEEE Trans. Antennas Propag.*, vol. 55, no. 5, pp. 1348–1358, May 2007.
[14] Y. Shi, H. G. Wang, L. Li, and C. H. Chan, "Multilevel Green's function interpolation method for scattering from composite metallic and dielectric objects," *J. Opt. Soc. Amer. A*, vol. 25, no. 25, pp. 2535–2548, 2008.
[15] M. D. Buhmann, *Radial Basis Functions: Theory and Implementations*. Cambridge, U.K.: Cambridge Press, 2003.

[16] Y. Shi and C. H. Chan, "Comparison of interpolating functions and interpolating points in full-wave multilevel Green's function interpolation method," *IEEE Trans. Antennas Propag.*, vol. 58, no. 8, pp. 2691–2699, Aug. 2010.
[17] Y. Shi and C. H. Chan, "Improved 3D full-wave multilevel Green's function interpolation method," *Electron. Lett.*, vol. 47, no. 3, pp. 174–175, 2011.
[18] B. Fornberg, E. Larsson, and N. Flyer, "Stable computations with Gaussian radial basis functions," *SIAM J. Sci. Comput.*, vol. 33, no. 2, pp. 869–892, 2011.
[19] C. J. Trahan and R. E. Wyatt, "Radial basis function interpolation in the quantum trajectory method: Optimization of the multi-quadric shape parameter," *J. Comput. Phys.*, vol. 185, no. 1, pp. 27–49, 2003.
[20] B. Fornberg, T. A. Driscoll, G. Wrights, and R. Charles, "Observations on the behavior of radial basis function approximations near boundaries," *Comput. Math. Appl.*, vol. 43, nos. 3–5, pp. 473–490, 2002.
[21] J. H. Halton, "On the efficiency of certain quasi-random sequences of points in evaluating multi-dimensional integrals," *Numer. Math.*, vol. 2, no. 1, pp. 84–90, 1960.
[22] P. Ylä-Oijala, M. Taskinen, and J. Sarvas, "Surface integral equation method for general composite metallic and dielectric structures with junctions," *Prog. Electromagn. Res.*, vol. 52, no. 3, pp. 81–108, 2005.
[23] P. Zhao, D. Q. Liu, and C. H. Chan, "A hybrid 2-D/3-D multilevel Green's function interpolation method for electrically large multilayered problems," *IEEE Trans. Antennas Propag.*, vol. 64, no. 9, pp. 3931–3942, 2016.
[24] K. B. Alici and E. Ozbay, "A planar metamaterial: Polarization independent fishnet structure," *Photon. Nanostruct.-Fundam. Appl.*, vol. 6, pp. 102–107, 2008.

PENG ZHAO (S'12–M'16) received the B.Eng. degree and M.Phil. degree from the Electronic Engineering Department, Zhejiang University, China, in 2006 and 2008, respectively, and the Ph.D. degree in electronic engineering from the City University of Hong Kong, China, in 2014. He is currently a Faculty Member with the Key Laboratory of RF Circuits and Systems of Ministry of Education, Microelectronics CAD Center, Hangzhou Dianzi University, Hangzhou, China. He is also with the State Key Laboratory of Millimeter waves, Southeast University, Nanjing, China. His research interests include computational electromagnetics and antennas.

CHI HOU CHAN (S'86–M'86–SM'00–F'02) received the B.S. and M.S. degrees in electrical engineering from The Ohio State University, Columbus, OH, USA, in 1981 and 1982, respectively, and the Ph.D. degree in electrical engineering from the University of Illinois at Urbana–Champaign, Urbana, IL, USA, in 1987.

From 1987 to 1989, he was a Visiting Assistant Professor with the Department of Electrical and Computer Engineering, University of Illinois. From 1989 to 1998, he was a Faculty Member with the Department of Electrical Engineering, University of Washington, Seattle, WA, USA. In 1996, he joined the Department of Electronic Engineering, City University of Hong Kong (CityU), and was promoted to the Chair Professor of Electronic Engineering in 1998. From 1998 to 2009, he was the first Associate Dean and then the Dean of the College of Science and Engineering. He also served as an Acting Provost with CityU from 2009 to 2010. He is currently the Director of the State Key Laboratory of Millimeter Waves, Partner Laboratory in CityU. His current research interests include computational electromagnetics, millimeter-wave circuits and antennas, and terahertz science and technology.

Dr. Chan received the U.S. National Science Foundation Presidential Young Investigator Award in 1991, the Joint Research Fund for Hong Kong and Macao Young Scholars, National Science Fund for Distinguished Young Scholars, China, in 2004, and outstanding teacher awards from the Department of Electronic Engineering, CityU, in 1998, 1999, 2000, and 2008. He is the General Co-Chair of ISAP 2010, iWAT2011, iWEN 2013, ICCEM 2015, and ICCEM 2016.

GAOFENG WANG (S'93–M'95–SM'01) received the Ph.D. degree in electrical engineering from the University of Wisconsin–Milwaukee, Milwaukee, WI, USA, in 1993, and the Ph.D. degree in scientific computing from Stanford University, Stanford, CA, USA in 2001. He is currently a Distinguished Professor with Hangzhou Dianzi University, Hangzhou, China. His current research interests include design, modeling, and the simulation of IC and MEMS.